A Rational Strategy for Graphene Transfer on Substrates with Rough Features

Jin-Yong Hong, Yong Cheol Shin, Ahmad Zubair, Yunwei Mao, Tomás Palacios, Mildred S. Dresselhaus, Sung Hyun Kim, and Jing Kong**

Since the successful isolation of an atomic layer graphene from its bulk in 2004,[1] tremendous knowledge and technology development has been made regarding this material. While chemical vapor deposition (CVD) synthesis using metal foils offers graphene material with high quality and on an industrial scale, transfer procedures are required to remove the underlying metallic substrates in order to use the graphene. For this purpose, a polymer supporting layer has been used, up to now.

Poly(methyl-methacrylate) (PMMA) has been the predominant choice until now due to its ease in handling and processing.[2] Nevertheless, the graphene transfer process using PMMA has not been completely satisfactory: the transferred graphene very often shows cracks and tears resulting from the transfer;[3] PMMA cannot be fully washed away with solvent,[4] and its residues tend to act as charge carriers scattering centers thereby degrading the electrical properties of the graphene.[5] Furthermore, it has been very challenging to transfer the graphene onto substrates with features such as terraces or grooves.

Consider, for example, the process of graphene being transferred to a substrate with surface features. Researchers have reported that the transferred graphene is often broken around those features.[6] In a typical PMMA-mediated wet-transfer process, a PMMA/graphene film is placed on a target substrate by being scooped in a DI (deionized) water bath and then is dried by compressed N_2. If there is a prepatterned structure with a certain aspect ratio on the substrate, then while the graphene region contacted on the horizontal side of the structure is dried, the side wall of the structure retains trapped water, making the PMMA/graphene sheet suspended. Tearing of graphene at these side wall regions has always been observed, possibly due to the large surface tension during the drying process, or due to the aggressively blowing N_2 to push the graphene/PMMA to lay conformally on the substrate. This difficulty of the graphene transfer limits the use of graphene in many important applications with uneven features in the topology.

In addition, wrinkles have been observed ubiquitously in CVD graphene, and studies have shown that these wrinkles are undesirable for carrier transport.[7] There might be various reasons for the wrinkle to form,[8] one most commonly considered is the fact that graphene has a negative coefficient of thermal expansion (CTE) while the underling metal substrates have a positive value.[9] Moreover, the wet-transfer process carried out in a DI water bath also creates additional wrinkles in the graphene when transferred onto a final target substrate (e.g., an SiO_2/Si wafer). It has been shown that wrinkles cause scattering of carriers (which reduce mobility) and the carbon atoms along the wrinkle are found to be less stable due to curvature effect.[10] It would therefore be highly desirable to have wrinkle-free graphene for future applications.[11]

For these reasons, a novel polymer, ethylene-vinyl acetate (EVA) is explored as a supporting layer for graphene transfer. It is found that the aforementioned challenging issues can be addressed by choosing an optimum correct polymer support layer for a particular application. This study shows that EVA consists of ethylene and vinylacetate units was such a polymer for many applications in our laboratory. EVA is lighter, more flexible, ease-stretchable, and less deformative than PMMA.[12] In addition, other properties, such as a higher thermal conductivity with higher CTE, lower glass transition temperature (T_g), lower elastic modulus, and high elongation capability, all contribute to making EVA an attractive candidate for the transfer supporting material. Furthermore, the better solubility of EVA than PMMA in solvents was expected to leave less residue on the graphene surface.

To demonstrate the generality and reliability of our graphene transfer method, two extreme cases were considered to verify and validate the EVA-supported graphene transfer method: One is "graphene transfer onto a rough substrate," and the other is "graphene transfer from a rough copper (Cu)." The transfer

Dr. J. -Y. Hong, A. Zubair, Prof. T. Palacios, Prof. J. Kong
Department of Electrical Engineering and Computer Science
Massachusetts Institute of Technology
77 Massachusetts Avenue, Cambridge
MA 02139, USA
E-mail: jingkong@mit.edu
Dr. Y. C. Shin
Department of Materials Science and Engineering
Massachusetts Institute of Technology
77 Massachusetts Avenue, Cambridge, MA 02139, USA
Y. Mao
Department of Mechanical Engineering
Massachusetts Institute of Technology
77 Massachusetts Avenue, Cambridge, MA 02139, USA
Prof. M. S. Dresselhaus
Department of Physics
Massachusetts Institute of Technology
77 Massachusetts Avenue, Cambridge, MA 02139, USA
Prof. S. H. Kim
Department of Chemistry
Seoul National University
599 Gwanak-ro, Gwanak-gu, Seoul 151-742, Korea
E-mail: shkim75@snu.ac.kr

DOI: 10.1002/adma.201505527

process was compatible with the established PMMA-supported transfer and the desired device properties of graphene using EVA as a supporting material was shown to have better quality than those properties when using PMMA.

For graphene to be transferred onto flat substrates, much effort has previously been made to avoid cracks or broken regions. It was commonly observed that if a certain region of graphene does not have good contact with the substrate, then that region very often will break after the PMMA is removed.[13] Therefore in order to have the graphene to be transferred successfully on to rough substrates with minimal broken regions, good conformal contact is essential. For this reason we concluded that preservation of good mechanical properties of the polymer/graphene layer is important for many applications.

It has been known that amorphous polymers (i.e., PMMA) are usually hard and brittle below their glass transition temperature because of the low mobility of their molecules, whereas the semi-crystalline polymers (i.e., EVA) with relatively strong intermolecular forces exhibit more rubber-like behavior, thereby providing elasticity and impact resistance.[14] We started our investigation by evaluating the elastic properties of the polymer/graphene layer.

Figure 1a shows the schematic diagram of our nanoindentation experiment,[15] with an atomic force microscope (AFM) tip at the center of the suspended polymer (PMMA or EVA) or polymer/graphene layer. A freely suspended EVA film revealed a substantial decrease in the elastic modulus (E) through load–displacement tests (Figure 1b). The elastic modulus of the suspended polymer film was obtained from the initial unloading contact stiffness, S, which is defined as

$$S = \mathrm{d}P / \mathrm{d}h \tag{1}$$

and is measured as the slope of the initial portion of the unloading curve. Based on Sneddon's theory,[16] the initial unloading contact stiffness can be derived as follows

$$S = 2\beta[(A/\pi)E_r]^{0.5} \tag{2}$$

where A is the contact area, β is a constant related to the geometry of the indenter (for a Berkovich indenter, $\beta = 1.034$), and E_r is the reduced elastic modulus. The quantity E_r can be calculated from the following equation

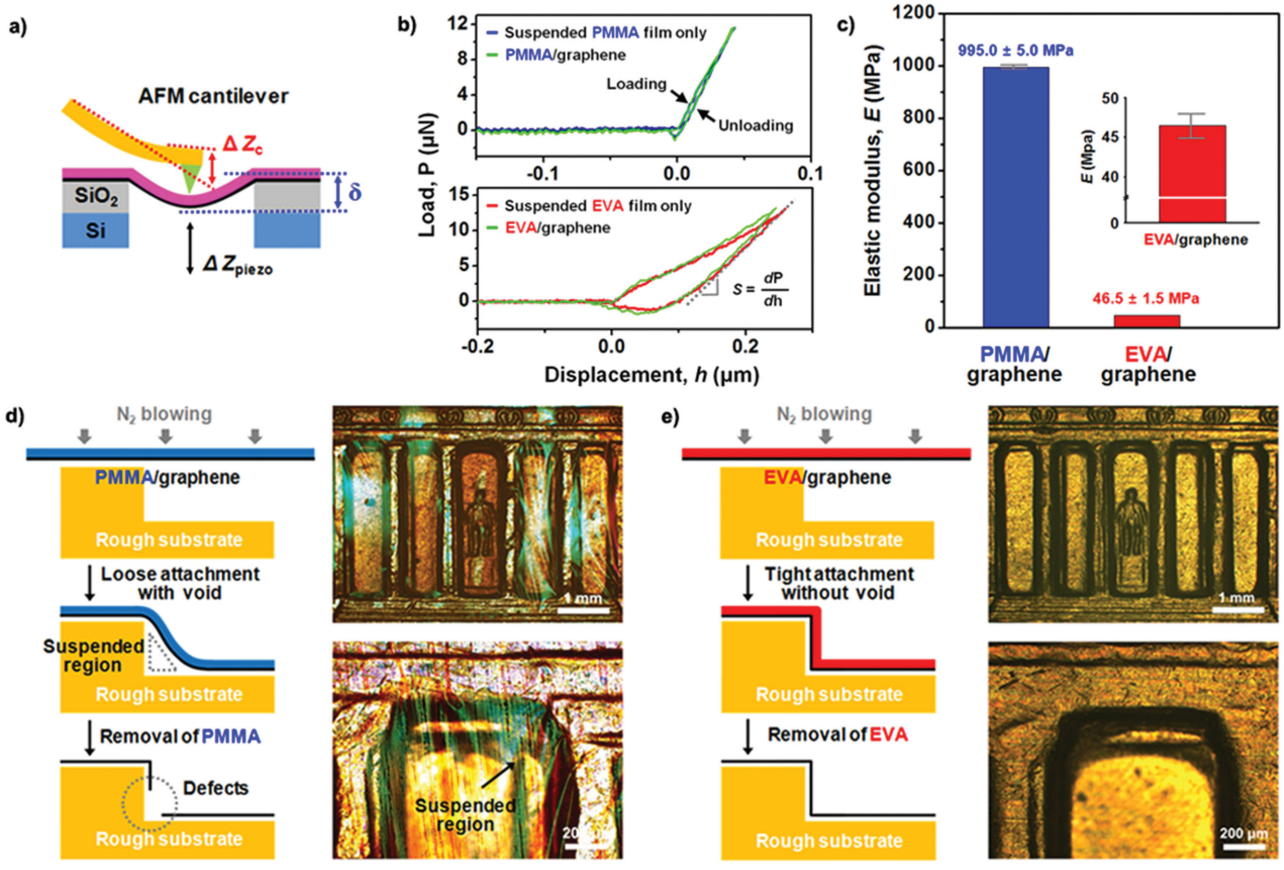

Figure 1. a) Schematic illustration of the bending test experiment carried out on a freely suspended sample. b) Representative load–displacement curves of nanoindentation for suspended polymer and polymer/graphene films (green line). The mechanical properties were characterized by a Digital Instrument Nanoscope IIIA from Veeco. A set of indentations were performed using calibrated silicon tips glued to Al-coated cantilevers with a spring constant of 80 N m^{-1} and a resonance frequency of 320 KHz. c) Elastic modulus values (E) for PMMA/graphene and EVA/graphene films. The indicated error bars of measurements are shown. d,e) Different behaviors in transfer process between d) PMMA/graphene and e) EVA/graphene during the transfer process. Back side of a coin (1 cent) was chosen for an arbitrary substrate. Schematic illustration representing the sequential steps for transferring graphene to an arbitrary substrate. The corresponding OM images were taken with ×25 (upper) and ×100 (lower) magnifications.

$$1/E_r = \left[\left(1-\nu^2\right)/E\right] + \left[\left(1-\nu_i^2\right)/E_i\right] \quad (3)$$

where E and ν are the elastic modulus and Poisson's ratio of the polymer films, respectively, and E_i and ν_i are the same quantities for the nanoindenter (E_i = 179 GPa, ν_i = 0.278). Assuming that the polymer/graphene film is a composite, we can predict the E values using the rule of mixtures.[17] Under our experimental condition, the E values of the polymer/graphene films were estimated as 995.0 ± 5.0 and 46.5 ± 1.5 MPa for the PMMA/graphene and EVA/graphene films, respectively (Figure 1c). Generally, the overall properties of the composite are dependent on the volume fraction of the components. In this polymer/graphene composite system, since the graphene is only 1 atomic layer in thickness, the volume fraction of the graphene is extremely small (<0.00003). Even though graphene has an extremely high E value (1 TPa),[18] the resulting E values of polymer/graphene film (Figure 1b green line) were almost the same as the those of polymer films alone, indicating that the mechanical property of the polymer is playing the dominant role in the polymer/graphene film. It should be noted that the approximately one-twentieth lower E value of the EVA/graphene film implies a tremendously lower stiffness in comparison with the PMMA/graphene film, and it is also anticipated that the EVA/graphene film would follow the surface of the underlying substrate much better and have a tighter attachment to the surface.

The influence of the mechanical properties of polymer support on the graphene transfer was investigated by using the back side of a one-cent U.S. coin (95% copper, 1962–1982 vintage) as an example of a rough substrate. Indeed, PMMA/graphene and EVA/graphene films exhibited quite different behaviors when transferred to such a coin. As can be seen in the optical microscopy (OM) image in Figure 1d, there are quite a lot unattached/suspended regions between the PMMA/graphene film and the features on the substrate (giving rise to a reflected greenish color). Thus, the PMMA/graphene film indeed does not make a conformal contact following the features on the substrate and the unattached/suspended regions will break easily either during or after the PMMA is being stripped away (as illustrated in the schematic explanation in Figure 1d). In contrast, as can be seen in the OM image of Figure 1e, the EVA/graphene film covers the surface of the side wall and made a tight contact without any unattached/suspended region, as anticipated. Such flexibility will be a great advantage for featured substrates (as shown in the schematic diagram in Figure 1e). Furthermore, two magnified OM images captured at different focal planes confirmed that the EVA/graphene film was completely attached to the substrate, as shown also in Figures S1 and S2 (Supporting Information).

To compare the actual transfer results with the theoretical predictions, a simulation was constructed and calculated based on a finite element analysis using the ABAQUS software. **Figure 2** shows the ABAQUS setups that have been used in the present study, where both the PMMA/graphene and EVA/graphene are transferred to a step edge (modeled as a plate with 200 μm in width and 50 μm in depth). We used this plane strain case capability to mimic the scenario in the experiment, with the long-distance along one direction of the slots in the coins. A very thin polymer/graphene film is placed exactly above the modeled plate. The thicknesses of the polymer/graphene films are set to be 0.3 and 1.0 μm for the PMMA and EVA, respectively (which correspond to the typical thicknesses of the two types of polymers when they are used for graphene transfer). The N_2 blowing pressure we used in the simulation is set to be 20 psi. Because the interaction between the polymer/graphene film and the coin is essentially not known, we consider a typical friction surface with a friction coefficient of 0.35. Even though the PMMA is an elastic–plastic polymer while the EVA is a viscoelastic material, in order to simplify the setup, we have assumed these two materials to have linear elastic and Young's modulus values set to be the values we obtained from our nanoindentation experiments. The main results are shown in the subsequent images, for PMMA and EVA, respectively. Obviously, even though the EVA is thicker, it can be closely attached to the plate while the PMMA cannot. Thus, the PMMA left some suspended part behind, which will damage the graphene during or after the polymer stripping process. It has been also known that fatigue crack (or fracture) growth is related to the residual stress level. Indeed, the stress distributions of the attached polymer/graphene films showed that the localized stress value of the EVA/graphene film was 2.27 MPa at the bottom corner of plate, which is 1/4 less than that of the PMMA/graphene film (10.02 MPa). This result is in good agreement with those obtained from the nanoindentation test. The EVA/graphene film exhibited a relatively low E value, which resulted in significantly lower residual stresses as compared to the PMMA/graphene film. Namely, the coordination between the higher elasticity and lower stiffness was found to play a pivotal role in the ability to transfer graphene successfully onto arbitrary substrates.

To further verify that the EVA-supported graphene transfer leads to a complete graphene layer on the coin substrate, an anticorrosion test was performed on the one-cent coin with 30% H_2O_2 as an oxidizing agent. If there are no cracks or broken region in the transferred graphene, the molecular diffusion barrier property of graphene's sp^2 honeycomb lattice was expected to prevent the Cu coin from leaching reactive chloride ions (Cl^-). After exposure to H_2O_2, a definite contrast arises between the graphene-coated and uncoated regions. The graphene-coated region (right) maintained its original appearance, whereas the uncoated region (left) showed a substantial darkening (Figure S3, Supporting Information). In addition, the X-ray photoelectron spectroscopy (XPS) survey spectrum reveals that the graphene-coated region in the inset of this figure exhibits two distinct Cu peaks at around 932.5 and 952.5 eV in the XPS spectrum (red trace), which correspond to the $Cu2p_{3/2}$ and $Cu2p_{1/2}$, respectively.

However, the uncoated region displays broader $Cu2p_{3/2}$ and $Cu2p_{1/2}$ XPS peaks, which can be attributed to the presence of copper oxides; Cu_2O (932.5 and 952.3 eV), CuO (933.6 and 953.4 eV), and $Cu(OH)_2$ (934.7 and 954.5 eV).[19] Furthermore, the several satellite peaks that are seen in the Cu 2p spectra (black trace in Figure S3, Supporting Information) provides definitive evidence for the presence of Cu^{2+} ions on the bare Cu coin surface.[20] These XPS data indicated that the EVA-transferred graphene indeed served as a diffusion barrier to protect the underlying Cu coin from oxidation. Such a test is a quick

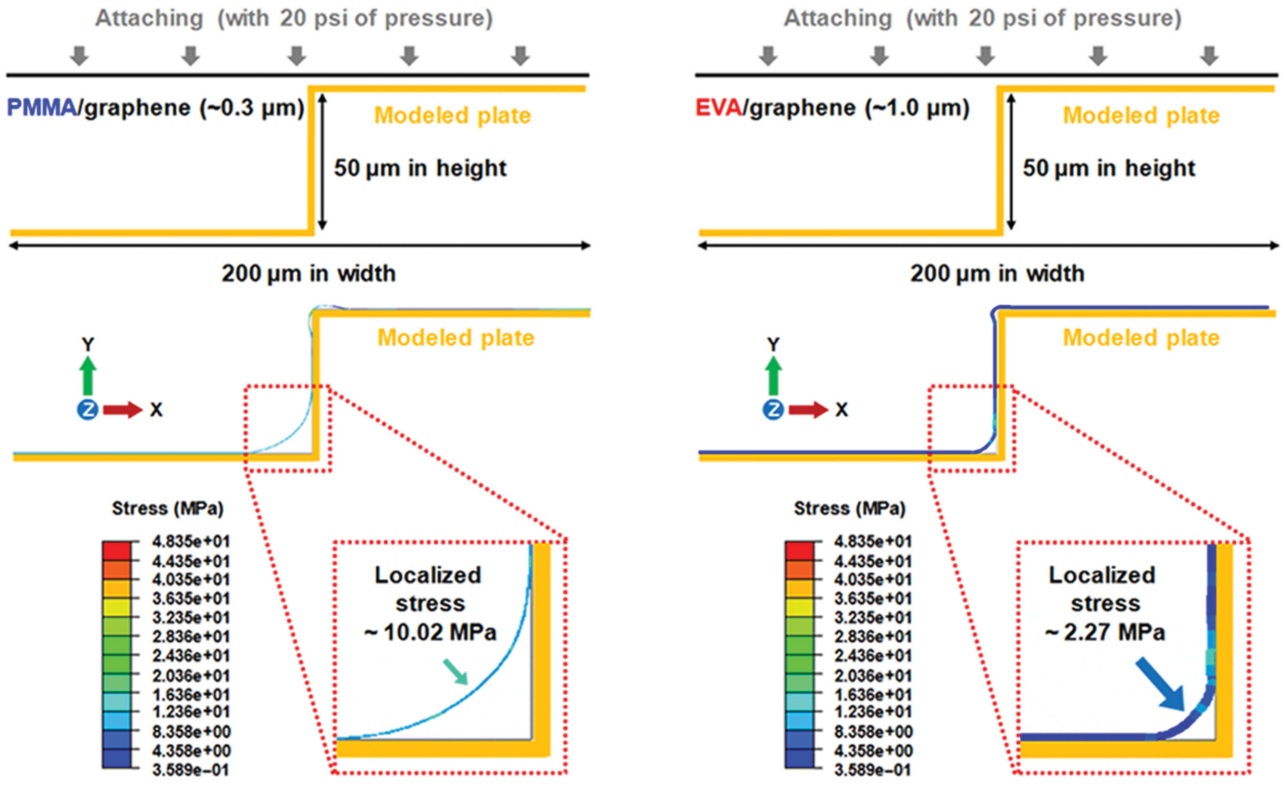

Figure 2. ABAQUS simulation analysis by using PMMA/graphene film (left) and EVA/graphene film (right). The part shown in the square is enlarged on the inset on the bottom. Insets show the normalized stress distributions of polymer/graphene films under a pressure of 20 psi.

way to verify that the EVA-transferred graphene is free from structural tears and broken regions over a large area.

The as-grown graphene on a flat Cu foil usually shows many wrinkles due to the differences between the CTE of graphene and that of metallic Cu. For a Cu substrate with additional features, the conformal graphene growth on that Cu substrate will result in even more corrugations in the graphene film. In order to obtain a transferred graphene with both minimal broken regions and minimal wrinkles, we have employed a novel hot-water bath transfer process in addition to using EVA as the polymer support. The overall procedures for transferring CVD grown graphene from textured Cu are illustrated in **Figure 3**a. Textures were obtained on a Cu foil simply by pressing the foil with a Fresnel lens as a mold (Figure S4, Supporting Information). Afterward resulting conformal graphene was grown on these textured 25 μm thick Cu foils (99.8%, Alfa Aesar) with concentric circle patterns (Figure S4b, Supporting Information) via a typical low-pressure chemical vapor deposition (LPCVD) process (Figure S5, Supporting Information). After the growth process, graphene is transferred onto the final target substrate through either the conventional polymer-assisted wet transfer approach or the new hot-water bath approach. The old approach is comprised of three essential steps; (1) the spin-coating of polymer support/carrier materials, (2) wet chemical etching of the Cu foil, and (3) transferring the graphene/polymer onto the target substrate and removal of the polymer.

The only difference between the "old" and "new" transfer procedure was in the third step. In a typical PMMA-mediated graphene transfer, a PMMA/graphene stack floats on the surface of a DI water bath at room temperature and the stack would be scooped out later, and finally transferred onto a target substrate. In contrast, for the new approach, an EVA/graphene stack is floated on the surface of hot DI water bath maintained at 90 °C for 1 h before scooping out (remaining procedures are the same as those previously used for the PMMA-supported method). During this period of the DI hot water bath, two things could happen: (1) since 90 °C is close to the melting temperature (T_m) of EVA, EVA might become liquid like and smoothed out on the graphene surface (**Table 1**); (2) the EVA layer should become isotropically expanded with the additional thermal energy. As a result, it can be anticipated that the wrinkles/corrugations in the graphene might be smoothed and stretched out. This allows the EVA/graphene stack to become tightly attached to the final substrate, thereby reducing the amount of wrinkles coming from the textured Cu foil. Consequently, it was expected that the graphene ripples which originated from the textured Cu could be lessened or eliminated during the transfer process through the flow and the isotropic expansion of EVA, whereas these ripples would have remained using the conventional PMMA-supported transfer.

Characterizations of graphene transferred by the two different techniques were carried out and the results were compared by OM, α-step profilometer as shown in Figure 3b. The OM image of the textured Cu exhibited well-defined concentric circle patterns, which replicate the features on the original lens. The height analysis in Figure 3b revealed that the wavelength and amplitude of the features on Cu before and after the growth

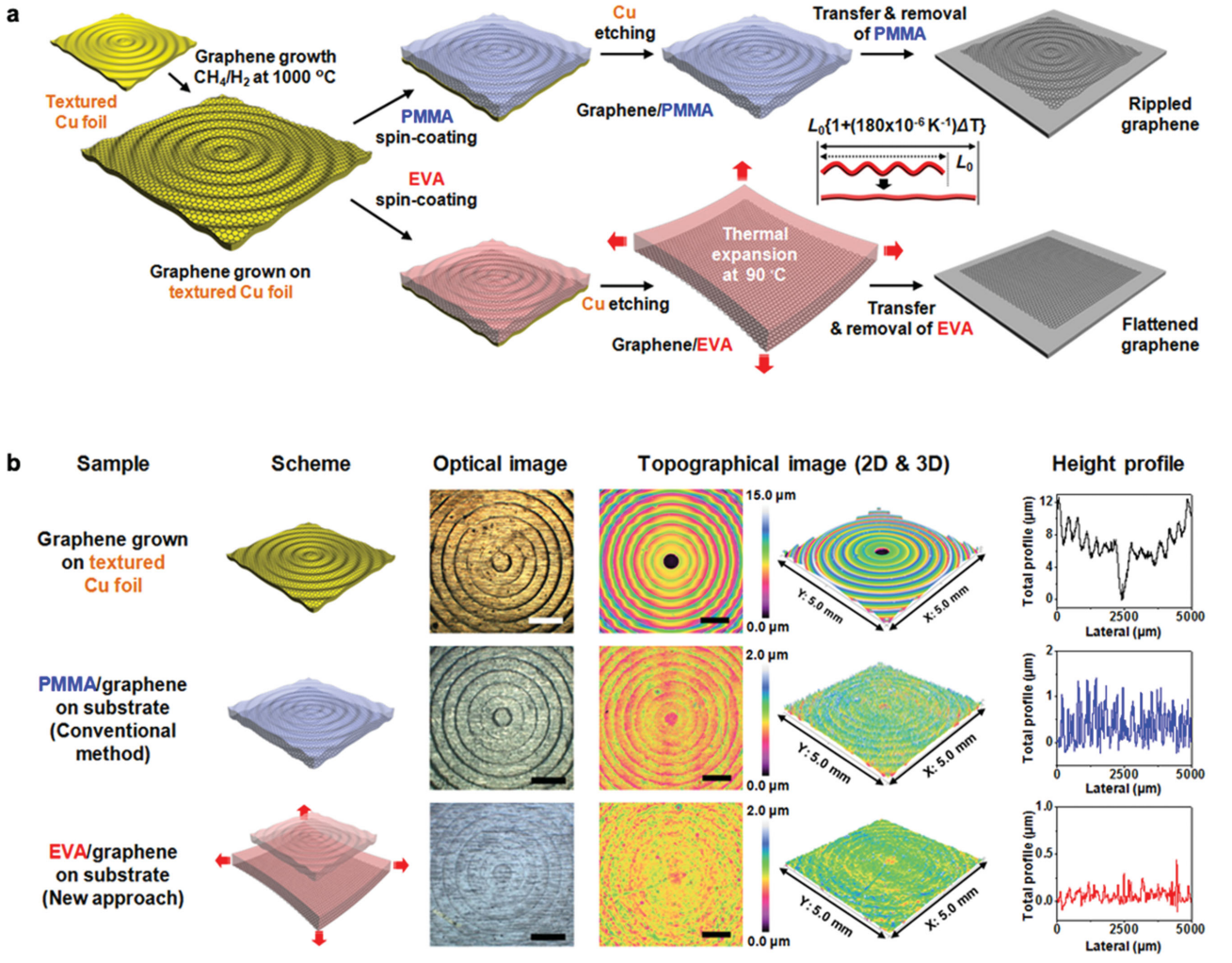

Figure 3. a) Schematic illustration of the different steps for transferring CVD graphene including polymer spin-coating, Cu etching, isotropic expanding, and transferring to target substrate. Graphene ripples generated by textured copper can be diminished by isotropic expansion of EVA (by heating to 90 °C) supporting material. b) Transfer results showing comparison between different support/carrier materials. The textured Cu foil with concentric circle patterns was prepared by pressing the Cu foil with a prepatterned mold. All graphic images and height analyses were taken before stripping off supporting materials from substrate. Scale bars in optical and topographical images are 1 mm.

were both ≈300 and 1.5 μm, respectively. With the conventional PMMA transfer method, these ripple (wavy) patterns were replicated and transferred to the final target substrate. The OM and topographical images show that identical patterns of the textured Cu still remained on the PMMA/graphene stack. The EVA/graphene transferred onto flat SiO_2/Si substrates, on the other hand, had much diminished patterns (Figure 3b and Supporting Information Figure S6), as revealed by the less color contrast in the OM and much reduced variation in the topographic height profile. The difference in height between the high and low patterns ranged from 0.1 to 0.2 μm in the EVA/graphene stack, which in comparison is much smoother than that of PMMA/graphene stack (ranging from 0.5 to 1.3 μm). Consequently, it was found that the macroscopic wrinkles from textured Cu could be reduced (or even removed) by introducing the EVA polymer as a support/carrier material. Further details of the mechanism and structural formation during transfer are discussed as below.

As mentioned earlier, our new graphene transfer with EVA exploits its thermal properties. In general, most solid materials expand upon heating and contract when cooled. The fractional change in length (l) with temperature (T) may be expressed as

$$(l_f - l_0)/l_0 = \alpha_l (T_f - T_0) \text{ or } \Delta l / l_0 = \alpha_l \Delta T \quad (4)$$

where l_0 and l_f are the initial and final lengths as the temperature is changed from T_0 to T_f, respectively. The parameter α_l is the linear CTE. This CTE value is a material property that is indicative of its ability of the material to increase its length as the result of an applied thermal energy. The thermal conductivity (κ) is also an important factor in heat transfer. Under our experimental conditions, the α_l and κ values were estimated using Equation (4) and Fourier's law, and the results are summarized in Table 1. It is known that a single graphene layer has negative CTE value. At room temperature (300 K), graphene exhibits an α_l value of approximately -7×10^{-6} K^{-1}, and α_l decreases

Table 1. Comparison of property parameters between PMMA and EVA films.

Sample	Mechanical properties[a)]		Physical and chemical properties					
	Contact stiffness [μN μm^{-1}]	Elastic modulus [GPa]	T_g [°C]	T_m [°C]	Thermal conductivity [W m^{-1} K^{-1}]	CTE value [×10^{-6} K^{-1}]	Molecular formula –	Solubility parameter[b)] [MPa$^{1/2}$]
PMMA	272.64	1.00	105	160	0.21[c)]	70[d)]	$(C_5O_2H_8)n$	18/19.7 (PMMA/Acetone)
EVA	94.06	0.05	61	87	0.34[c)]	180[e)]	$(C_2H_4)n$ $(C_4H_6O_2)m$	18.05/18.2 (EVA/Xylene)

[a)]The mechanical properties were characterized by a Digital Instrument Nanoscope IIIA from Veeco. A set of indentations were performed using calibrated silicon tips glued to Al-coated cantilevers with a spring constant of 80 N m^{-1} and a resonance frequency of 320 KHz; [b–e)]Values were collected from refs. [33–35] and [36], respectively.

with increasing temperature.[9] In this study, the variation of the graphene's CTE value in the temperature range of interest was found to be negligible. It is worth noting that the α_l value for EVA is ≈2.6 times higher than that of PMMA. Therefore, while the PMMA was dilated to $l_0(1+(70 \times 10^{-6}\ K^{-1})\Delta T)$ at a given temperature, the EVA expanded to $l_0(1 + (180 \times 10^{-6}\ K^{-1})\Delta T)$ at a given temperature, which is more than twice the expansion of PMMA. It was also expected that the good thermal conductivity (0.34 Wm^{-1} K^{-1}) and the relatively high CTE value (180×10^{-6} K^{-1}) of EVA would have a combined or synergistic effect on the isotropic expansion of EVA during the transfer process.

The schematic diagrams in **Figure 4**a,b depict the likely scenarios for the old and new transfer approaches. With the conventional PMMA-supported graphene transfer, the wrinkled or folded graphene regions due to the features on the Cu growth substrate would not make a tight contact with the target substrate (Figure 4a). This will give rise to voided regions in the graphene and therefore, broken regions were observed after the PMMA stripping, as shown in the OM in Figure 4c. On the other hand, the EVA/graphene film expanded in response to the increased temperature, and the wavy patterned EVA/graphene film could be flattened and transferred with much better contact to the final substrate (Figure 4b). Indeed, as shown in the OM image in Figure 4d, a clean and continuous transferred graphene surface without broken regions are observed for the EVA/graphene film.

The isotropic expansion, of course, could be applied to the conventional PMMA-supported transfer. The applied thermal energy also has an influence on the PMMA/graphene film, but their length change by thermal expansion is insignificant (Figure S7, Supporting Information).

This effect is further demonstrated in an extreme scenario as shown in **Figure 5**, where the two approaches are compared when a crumpled Cu foil is used as a growth substrate for graphene. Photographs and OM images revealed excellent continuity over a millimeter-sized length scale, without observable cracks or tears in the graphene transferred by EVA using the new hot-water bath approach, while the conventional transfer approach using PMMA resulted in a severely broken graphene film.

The residues of the support/carrier material, especially polymer residues of PMMA, inevitably remained on the graphene surface and adversely affected the graphene's intrinsic electrical properties.[8–10] Apart from the advantageous mechanical properties of EVA, its physical/chemical properties also result in less residue on the graphene which could be intended for device applications. The chemical parameters of a polymer in a solvent, including the intermolecular interaction, chain conformation, and solubility, are strongly affected by the inherent properties of the polymer as well as the environmental conditions where the polymer is used. In particular, the solubility parameter (δ) could be considered as an important factor in determining the dissolution efficiency of the support/carrier material.[21]

The Hildebrand–Scatchard equation is an equation for calculating the enthalpy change (ΔH_m) for the polymer–solvent mixing system, and can be expressed as

$$\Delta H_m = V_m \left(\delta_p - \delta_s\right)^2 \phi_p \phi_s \tag{5}$$

where V_m is the volume of the mixture, δ_p and δ_s are the solubility parameters, and ϕ_p and ϕ_s are the volume fraction of the polymer and solvent, respectively. For a polymer to be soluble in a solvent, the change in the Gibbs free energy of mixing (ΔG_m) must be negative (favorable), in accordance with the following basic thermodynamic equation

$$\Delta G_m = \Delta H_m - T\Delta S_m \tag{6}$$

where T is the temperature and the ΔS_m is the entropy of mixture. The ΔS_m term is usually positive, and thus, ΔH_m is the determining factor. Since $\Delta H_m \approx (\delta_p - \delta_s)^2$, the highest solubility is achieved when the δ_p and δ_s values are equal, due to a negative entropy term. Namely, mixtures of materials with similar δ values are likely to be miscible and thermodynamically compatible.

Acetone is the most widely used solvent for dissolving/removing of PMMA. From Table 1, the PMMA has a solubility parameter of about 18 MPa$^{1/2}$, and the solubility parameter difference ($|\delta_{PMMA} - \delta_{Acetone}|$) is 1.7. In the case of EVA (δ_p value of 18.05 MPa$^{1/2}$), however, the acetone is not a suitable solvent due to the solubility parameter mismatch. It has been known that an aromatic hydrocarbon, such as xylene, is a more suitable solvent for dissolving/removing EVA.[22] For this study, the xylene with a δ_s value of 18.2 MPa$^{1/2}$ was chosen to promote a more effective removal of EVA residues from the graphene surface. The $|\delta_{EVA} - \delta_{Xylene}|$ value is revealed to be 0.15, indicating that xylene is "better solvent" for EVA (Table 1). Thus it is anticipated that the interactions between the EVA polymer and the xylene solvent should be energetically favorable to allow the solvent swell of the EVA polymer chains to dissolve away from the graphene surface more effectively.

Figure 6a,b shows the OM images of graphene on SiO_2/Si substrates obtained by the conventional PMMA-supported transfer process (Figure 6a; here PMMA was removed by acetone)

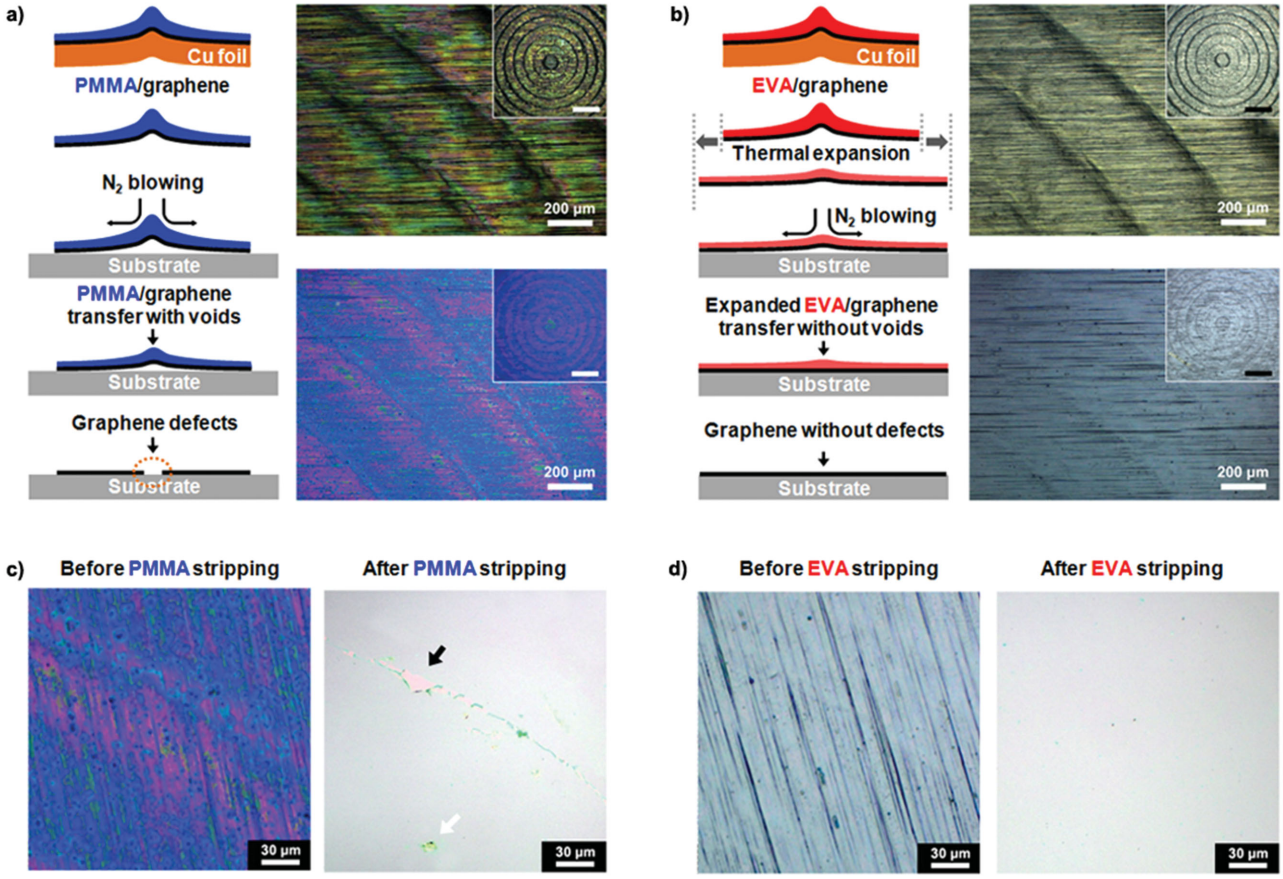

Figure 4. a,b), Comparison of thermal expansion effects between a) PMMA/graphene and b) EVA/graphene during the transfer process. Schematic illustration representing the sequential steps of graphene transfer from a rough Cu foil. The OM images depict spin-coated polymer on the rough Cu foil (upper) and attaching the polymer/graphene film onto a SiO_2/Si wafer (lower) (inset: low-magnification images. Scale bar is 1 mm). c,d) The OM image of the transferred polymer/graphene film before/after the c) PMMA and d) EVA stripping. Structural defects on the transferred graphene were observed after the PMMA stripping (black arrow). The graphene surface after stripping off the PMMA also shows some polymer residue of the PMMA (white arrow).

and the hot-water bath EVA transfer process (Figure 6b; here EVA was removed by xylene). White arrows in Figure 6a indicate that the PMMA residues on graphene are typically observed, while for the EVA case such residues can hardly be found. Furthermore, wrinkles can be clearly seen in the PMMA-transferred graphene (black arrow in Figure 6b), but are much less frequently seen in the hot-water bath EVA-transferred graphene.

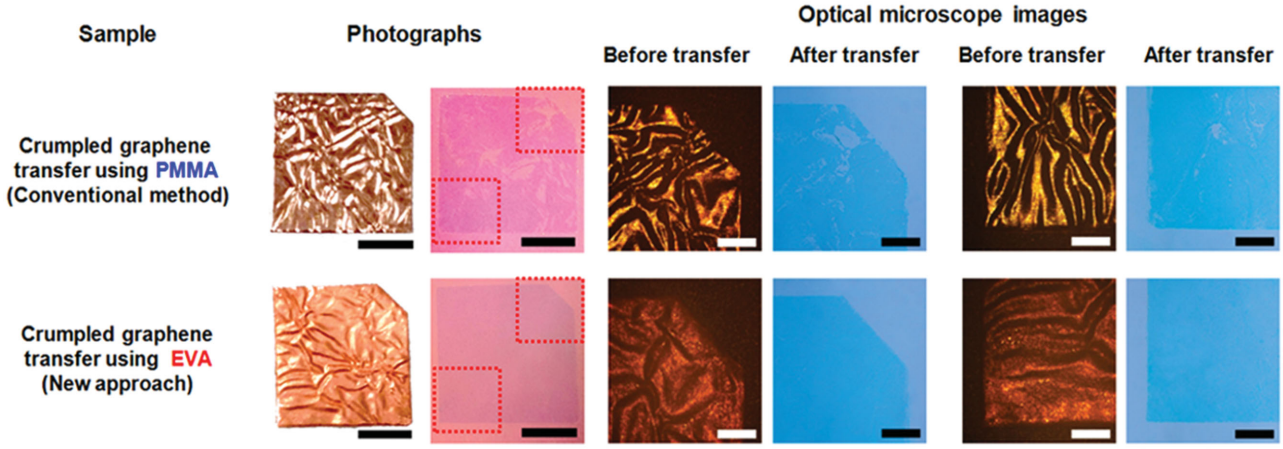

Figure 5. Photographs of graphene grown on a crumpled Cu foil (scale bar is 3.5 mm), and the corresponding OM images of the transferred graphene (scale bar is 1 mm). Graphene transferred on a SiO_2/Si wafer using PMMA (top) and EVA (bottom) as a support/carrier material.

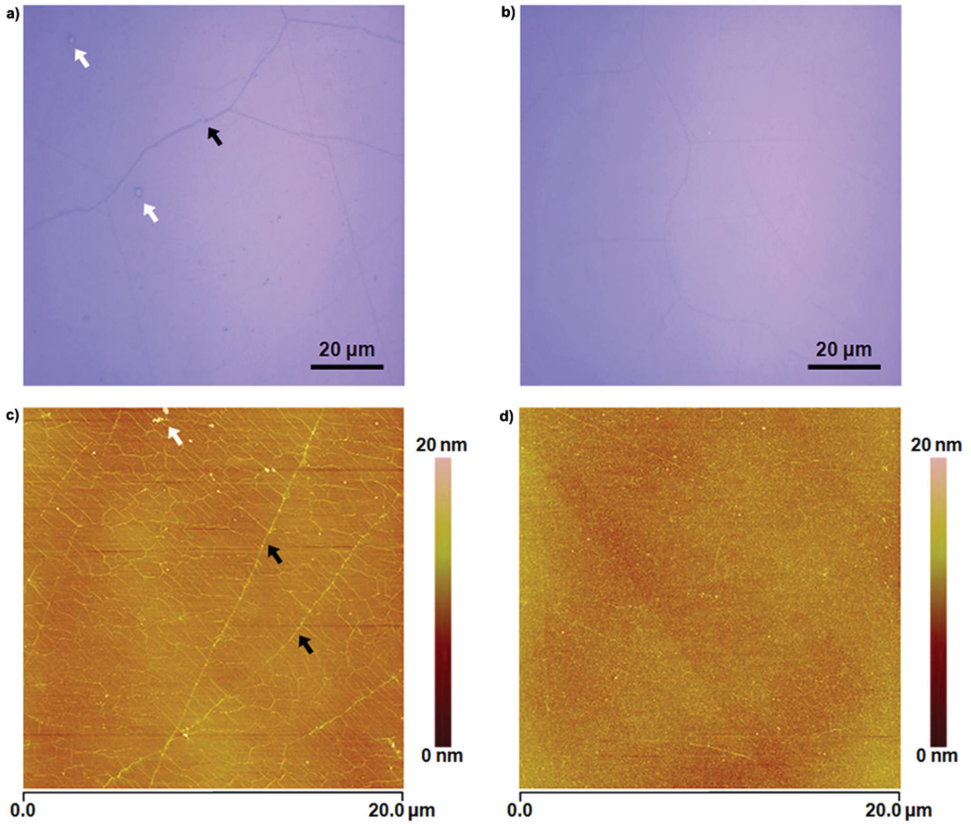

Figure 6. a,b) The OM images of monolayer graphene transferred to 300 nm SiO_2/Si substrate by using the a) PMMA-supported and b) EVA-supported transfer methods. While the graphene transferred by PMMA showed distinct wrinkles (black arrows) and residues (white arrow), a nicely clean surface was observed in the graphene transferred by EVA. c,d) The AFM images of graphene transferred to a 300 nm SiO_2/Si substrate by using the c) PMMA-supported and d) EVA-supported transfer methods.

AFM images also confirmed these observations at the nanometer-sized scale. Figure 6c is the AFM image of a graphene sample on SiO_2/Si transferred by the conventional PMMA method, a high density of graphene wrinkles (black arrows) and PMMA residues (white arrows) can be observed. In contrast, for the graphene transferred by the hot-water bath method with EVA, a significant reduction in the graphene wrinkle density and contaminant residues can be observed (Figure 6d). Although the EVA residue can be greatly reduced due to energetically favorable reaction, some EVA residues on graphene surface could possibly still exist. The OM and AFM images suggest that the EVA-transferred graphene has a much more uniform morphology with less contamination than the graphene films transferred by PMMA.

To compare the quality of the transferred graphenes, Raman spectroscopy characterization (532 nm laser wavelength) was first performed before electrical characterization, as shown in **Figure 7**a. It is clear that the both graphene samples have a typical monolayer graphene Raman spectrum with the G- and 2D-bands at 1590 and 2675 cm^{-1}, exhibiting a ratio of integrated peak intensities (I_{2D}/I_G) of larger than 5.0.[23] There is no significant difference in the ω_G and I_{2D}/I_G values between two samples. Nonetheless, the integrated intensity ratio between D and G peak (I_D/I_G) of the EVA-transferred graphene was negligible below the Raman detection limit, while that of the PMMA-transferred graphene was around 0.13, presumably due to the presence of the PMMA residues (Figure 7a, inset). This characterization suggested that the EVA-supported transfer method is relatively beneficial to minimize the creation of defects in the graphene during the transfer process.

Taking full advantage of the hot-water bath EVA-supported transfer method, the electrical properties of two different types of graphenes were investigated using a back-gated graphene field-effect transistor (GFET) device. Figure 7b is a top-view OM image of the back-gated graphene FET with a channel length (L) of 65 μm and width (W) of 25 μm. The p-type SiO_2/Si wafer serves as a back gate for the GFET, and Ti/Au source and drain pads were formed by photolithography. All the measurements were carried out in ambient air at RT. Compared with the GFET based on graphene transferred by PMMA, the graphene transferred by EVA exhibits lower sheet resistances with a narrower distribution. The graphene samples transferred with the EVA supporting layer method exhibit an average sheet resistance (R_s) of 366.8 ± 82.9 Ω sq^{-1}, lower than that of PMMA (460.5 ± 132.1 Ω sq^{-1}). The carrier mobility could be extracted from the sheet resistance by using the simple Drude model.[24] Since polycrystalline graphene samples grown by the Cu-mediated LPCVD process were used for the fabrication, the carrier mobility values themselves were not so high as the exfoliated graphene samples from natural

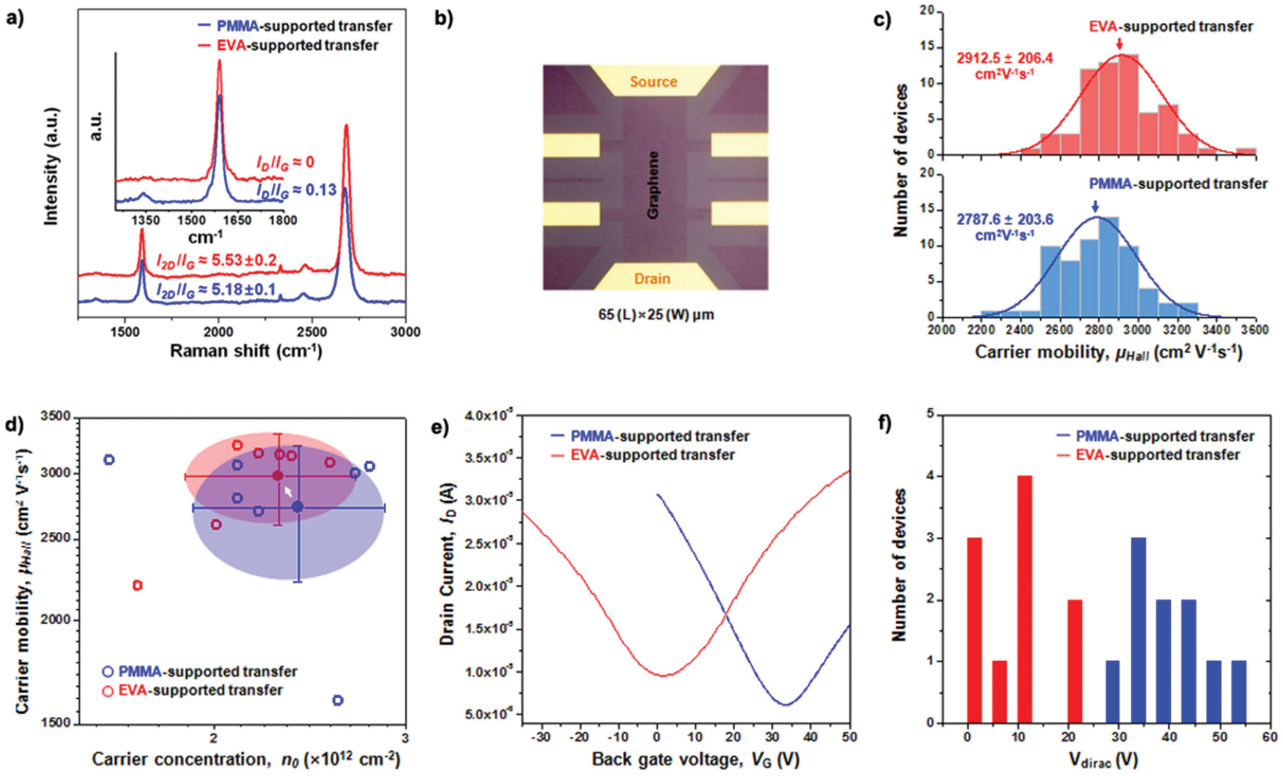

Figure 7. a) 532 nm excited Raman spectra of graphene transferred using PMMA (blue) and EVA (red) as supporting materials. The positions of I_D/I_G and I_{2D}/I_G of each sample are labeled together, respectively. b) The OM image of the back-gated graphene field-effect transistor. c) The carrier mobility distribution of graphene samples transferred by the PMMA-supported (blue) and EVA-supported (red) methods. d) Relation between the carrier concentration and the carrier mobility. The blue and red points and circles are for devices fabricated by PMMA and EVA-supported transferred graphenes, respectively. e) Drain current–back gate voltage (I_D–V_G) curves for the GFET samples transferred by the PMMA-supported (blue) and the EVA-supported (red) methods. f) Dirac point voltage (V_{Dirac}) for ten GFET samples transferred by the PMMA-supported (blue) and the EVA-supported (red) methods. All electrical measurements were carried out under environments of ambient air at RT.

graphite and HOPG.[25] Nonetheless, compared with the GFET based on graphene transferred by PMMA, the graphene transferred by EVA exhibits a slightly higher carrier mobility (μ_{Hall}). Figure 7c depicts the distribution of the μ_{Hall} of GFET devices (total ≈60 devices). A Gaussian fit indicates the carrier mobility values of 2912.5 ± 206.4 and 2787.6 ± 203.6 cm^2 V^{-1} s^{-1} for graphenes transferred by EVA and PMMA, respectively. Besides the sheet resistance and carrier mobility, carrier concentration (n_0) is also a parameter of concern in GFET devices, since n_0 reflects the degree of charge impurity scattering.[26] It can be seen that the EVA-supported transfer method gave rise to a decreased carrier concentration and an increased carrier mobility as shown in Figure 7d. Under our experimental condition, the n_0 values in Figure 7d were found to be $2.3 \times 10^{12} \pm 0.5$ and $3.8 \times 10^{12} \pm 1.5$ cm^{-2} for graphenes transferred by EVA and PMMA, respectively.

Figure 7e shows representative current–voltage (I_D–V_G, I_D is the drain current and V_G is the gate voltage) curves for the GFETs. The I_D–V_G curve of the GFET transferred by the PMMA-supported transfer method displays a further shifted Dirac point voltage (V_{Dirac}) than the EVA transferred graphene. Figure 7f summarizes the results for the devices tested. The average V_{Dirac} were 11.5 ± 8.0 V and 38.6 ± 7.1 V for the GFETs transferred by EVA and PMMA, respectively. Generally, the V_{Dirac} value depends on several factors: the charge transfer doping from the H_2O/O_2 molecules,[27] the metal contact effects,[28] and an increase of the external scattering sites due to polymer residue.[29] Under our experimental conditions, all devices were prepared at the same time to avoid interference from additional doping effects. Thus, we speculate that the tendency to the positive shift of V_{Dirac} might be due to the existence of PMMA residue (but with a substantially reduced polymer residue on the EVA graphene), since everything else is same for both devices. Physisorbed molecules on the graphene surfaces impact the electrical properties and alter the electronic structure of graphene. It has also been reported that a thin PMMA layer left on the graphene is reported to cause a p-type doping behavior in GFETs.[30] Furthermore, the fact that EVA graphene samples have a considerably lower wrinkle density could be attributed to the higher mobility and the decreased R_s in those samples.

In conclusion, as an alternative supporting material for graphene transfer, EVA was explored to tackle the challenging issues now found in the established PMMA-supported transfer process. It was found that EVA's excellent materials properties not only enable a conformal transfer onto uneven substrates without damaging the graphene continuity, but also result in much less residue on the graphene after transfer. With a novel hot-water bath expansion approach, the density of the wrinkles or folds in the graphene is much reduced, which also enables

a more successful transfer of graphene from a rough Cu substrate. Although this work only investigated the transfer of graphene from one substrate to another, it is anticipated that the use of EVA as a support/carrier material will contribute to the technological development of effective transfer methods for other 2D materials (i.e., h-BN, MoS_2, $MoSe_2$, WS_2, WSe_2) as well.

Experimental Section

Graphene Synthesis: High-quality monolayer graphene was grown on 25 μm thick Cu foils (99.8%, Alfa Aesar) using an LPCVD method that was demonstrated previously.[31] Before the CVD growth, the Cu foils were treated with the commercial Ni etchant (Nickel Etchant TFB, Transense) to allow reproducible synthesis of clean and continuous monolayer graphene.[32] After the precleaning process, the various types of Cu foils (flat, textured, crumpled) were loaded into a CVD chamber. Under low pressure (1.5 Torr), the textured Cu foil was annealed in a gas flow of 50 standard cubic centimeters (sccm) of hydrogen (H_2) at 1000 °C for 60 min. After the annealing step, 6 sccm of methane (CH_4) gas was introduced to initiate the graphene growth, for 40 min. The graphene growth was carried out at 1000 °C. To control the graphene growth rate, 20 sccm of H_2 flow was used during the growth period. Once the graphene growth was finished, the CVD chamber was cooled down under 20 sccm of H_2 to prevent oxidation and to minimize hydrogenation reactions of the graphene.

PMMA-Supported Graphene Transfer: After graphene growth, a PMMA solution (PMMA, 950 A9, MicroChem, diluted to 4.5 wt% in anisole) was spin coated onto the top side of the sample at 2500 rpm for 60 s and dried for 15 min in an oven held at 80 °C. Before the Cu etching process, the back-side graphene was removed by oxygen plasma etching for 3 min at a plasma power of 100 W. Copper etchant (CE-100, Transene Company Inc.) was used to etch Cu foil, and the PMMA/graphene film was floated on the surface of the solution. The PMMA/graphene film was moved to distilled water several times to rinse the etchant residue. After rinsing the PMMA/graphene film with distilled water, the PMMA/graphene film was placed on a target substrate (300 nm SiO_2/Si wafer) by being scooped out at room temperature and then was dried by compressed N_2. After blowing the compressed N_2, the sample was dried in an oven at 80 °C for several hours to enable the complete evaporation of moisture from the sample. Acetone was used to selectively remove the PMMA from the PMMA/graphene/SiO_2/Si wafer. The PMMA was removed by soaking the sample in an acetone bath overnight and dried in air.

EVA-Supported Graphene Transfer: After graphene growth, an EVA solution (Aldrich, vinyl acetate 18 wt%, 10 wt% dissolved in xylene) was spin coated onto the top side of the sample at 4000 rpm for 60 s and dried in an oven at 80 °C for 60 min. For the EVA-supported graphene transfer, the overall processes were the same as the above procedure except for the final step (transferring EVA/graphene onto the target substrate and removal of EVA). To give a thermal expansion of EVA layer, the EVA/graphene film in a distilled water bath was kept at 90 °C for 1 h before scooping out the film. Subsequently, the EVA/graphene/ 300 nm SiO_2/Si wafer was dried in an oven at 80 °C for several hours to enable the complete evaporation of moisture from the sample. The xylene was used to selectively remove the EVA. The EVA was dissolved and washed out by soaking the film in a boiling xylene bath for 15 min and the film was then dried in air.

Device Preparation and Electrical Performance Measurements: For the back-gated GFET devices, the metallization with Ti/Au layer was implemented on the graphene by evaporation and a subsequent lift-off process, after the patterning was accomplished by using e-beam lithography Elionix (ELS-F125). O_2/He plasma was used to pattern the graphene channels. Sixty back-gated GFET devices were thus fabricated where the channel length and width were 65 and 25 μm, respectively. All the electrical performance data in the main text were measured with Agilent 4155 Parameter Analyzer in ambient air at room temperature.

Characterizations: The morphology was confirmed using an Optical Microscopy (Zeiss Primo Star Microscope, Carl Zeiss). The surface profile was taken by using a P-16 Surface Profilometer (KLA-Tencor). The Raman measurement was carried out using a Horiba-Jobin Yvon system with a 532 nm Ar+ laser line. The laser power used was around 1 mW on the sample and a 100× objective was used to focus the beam. The size of the laser beam on the sample was around 1 μm. The mechanical properties of the films were characterized by a Digital Instrument Nanoscope IIIA from Veeco. A set of indentations was performed using calibrated silicon tips glued to Al-coated cantilevers with a spring constant of 80 N m^{-1} and a resonance frequency of 320 KHz.

Supporting Information

Supporting Information is available from the Wiley Online Library or from the author.

Acknowledgements

J.-Y.H. and Y.C.S. contributed equally to this work. This research was supported by the STC Center for Integrated Quantum Materials (CIQM) from NSF (US) grant DMR-1231319, Army Research Office (ARO) (Grant Nos. W911NF-14-2-0071, 6930265, and 6930861), the Electronic and Photonic Materials Program (EPM) and Condensed Matter Physics Program (CMP) (NSF/DMR 1507806), and Mid-career Research Program (NRF-2015R1A2A2A04006172) through NRF grant funded by the Ministry of Education, Science and Technology (MEST, Korea).

Received: November 9, 2015
Revised: December 2, 2015
Published online: January 25, 2016

[1] K. S. Novoselov, A. K. Geim, S. V. Morozov, D. Jiang, Y. Zhang, S. V. Dubonos, I. V. Grigorieva, A. A. Firsov, *Science* **2004**, *306*, 666.

[2] a) Z. Yan, J. Lin, Z. Peng, Z. Sun, Y. Zhu, L. Li, C. Xiang, E. L. Samuel, C. Kittrell, J. M. Tour, *ACS Nano* **2012**, *6*, 9110; b) N. Liu, L. Fu, B. Dai, K. Yan, X. Liu, R. Zhao, Y. Zhang, Z. Liu, *Nano Lett.* **2011**, *11*, 297; c) P. Gupta, P. D. Dongare, S. Grover, S. Dubey, H. Mamgain, A. Bhattacharya, M. M. Deshmukh, *Sci. Rep.* **2014**, *4*, 3882.

[3] a) X. Li, W. Cai, J. An, S. Kim, J. Nah, D. Yang, R. Piner, A. Velamakanni, I. Jung, E. Tutuc, S. K. Banerjee, L. Colombo, R. S. Ruoff, *Science* **2009**, *324*, 1312; b) X. Li, Y. Zhu, W. Cai, M. Borysiak, B. Han, D. Chen, R. D. Piner, L. Colombo, R. S. Ruoff, *Nano Lett.* **2009**, *9*, 4359.

[4] a) M. Her, R. Beams, L. Novotny, *Phys. Lett. A* **2013**, *377*, 1455; b) X. Liang, B. A. Sperling, I. Calizo, G. Cheng, C. A. Hacker, Q. Zhang, Y. Obeng, K. Yan, H. Peng, Q. Li, X. Zhu, H. Yuan, A. R. H. Walker, Z. Liu, L. Peng, C. A. Richter, *ACS Nano* **2011**, *5*, 9144.

[5] a) M. Jang, T. Q. Trung, J.-H. Jung, B.-Y. Kim, N.-E. Lee, *Phys. Chem. Chem. Phys.* **2014**, *16*, 4098; b) J. H. Chen, C. Jang, S. Xiao, M. Ishigami, M. S. Fuhrer, *Nat. Nanotechnol.* **2008**, *3*, 206.

[6] a) Y.-C. Lin, C. Jin, J.-C. Lee, S.-F. Jen, K. Suenaga, P.-W. Chiu, *ACS Nano* **2011**, *5*, 2362; b) J. Song, F.-Y. Kam, R.-Q. Png, W.-L. Seah, J.-M. Zhuo, G.-K. Lim, P. K. H. Ho, L.-L. Chua, *Nat. Nanotechnol.* **2013**, *8*, 356; c) W. Regan, N. Alem, B. Alemán, B. Geng, Ç. Girit, L. Maserati, F. Wang, M. Crommie, A. Zettl, *Appl. Phys. Lett.* **2010**, *96*, 113102; d) S. Gorantla, A. Bachmatiuk, J. Hwang, H. A. Alsalman, J. Y. Kwak, T. Seyller, J. Eckert, M. G. Spencere, M. H. Rümmeli, *Nanoscale* **2014**, *6*, 889; e) J. D. Caldwell,

T. J. Anderson, J. C. Culbertson, G. G. Jernigan, K. D. Hobart, F. J. Kub, M. J. Tadjer, J. L. Tedesco, J. K. Hite, M. A. Mastro, R. L. Myers-Ward, C. R. EddyJr., P. M. Campbell, D. K. Gaskill, *ACS Nano* **2010**, *4*, 1108; f) A. Reina, X. Jia, J. Ho, D. Nezich, H. Son, V. Bulovic, M. S. Dresselhaus, J. Kong, *Nano Lett.* **2009**, *9*, 30; g) J. W. Suk, A. Kitt, C. W. Magnuson, Y. Hao, S. Ahmed, J. An, A. K. Swan, B. B. Goldberg, R. S. Ruoff, *ACS Nano* **2011**, *27*, 6916.

[7] a) J. C. Koepke, J. D. Wood, D. Estrada, Z.-Y. Ong, K. T. He, E. Pop, J. W. Lyding, *ACS Nano* **2013**, *7*, 75; b) W. Zhu, T. Low, V. Perebeinos, A. A. Bol, Y. Zhu, H. Yan, J. Tersoff, P. Avouris, *Nano Lett.* **2012**, *12*, 3431.

[8] V. E. Calado, G. F. Schneider, A. M. M. G. Theulings, C. Dekker, L. M. K. Vandersypen, *Appl. Phys. Lett.* **2012**, *101*, 103116.

[9] a) D. Yoon, Y.-W. Son, H. Cheong, *Nano Lett.* **2011**, *11*, 3227; b) M. Z. Islam, M. Mahboob, R. L. Lowe, *J. Phys. D: Appl. Phys.* **2014**, *47*, 409501; c) W. Bao, F. Miao, Z. Chen, H. Zhang, W. Jang, C. Dames, C. N. Lau, *Nat. Nanotechnol.* **2009**, *4*, 562; d) A. Fasolino, J. H. Los, M. I. Katsnelson, *Nat. Mater.* **2007**, *6*, 858.

[10] X. Li, C. W. Magnuson, A. Venugopal, J. An, J. W. Suk, B. Han, M. Borysiak, W. Cai, A. Velamakanni, Y. Zhu, L. Fu, E. M. Vogel, E. Voelkl, L. Colombo, R. S. Ruoff, *Nano Lett.* **2010**, *10*, 4328.

[11] a) L. Gao, G.-X. Ni, Y. Liu, B. Liu, A. H. C. Neto, K. P. Loh, *Nature* **2014**, *505*, 190; b) D. Q. McNerny, B. Viswanath, D. Copic, F. R. Laye, C. Prohoda, A. C. Brieland-Shoultz, E. S. Polsen, N. T. Dee, V. S. Veerasamy, A. J. Hart, *Sci. Rep.* **2014**, *4*, 5049; c) D. Ma, Y. Zhang, M. Liu, Q. Ji, T. Gao, Y. Zhang, Z. Liu, *Nano Res.* **2013**, *6*, 617; d) W.-H. Lin, T.-H. Chen, J.-K. Chang, J.-I. Taur, Y.-Y. Lo, W.-L. Lee, C.-S. Chang, W.-B. Su, C.-I. Wu, *ACS Nano* **2014**, *8*, 1784.

[12] a) B. N. Chandrashekar, B. Deng, A. S. Smitha, Y. Chen, C. Tan, H. Zhang, H. Peng, Z. Liu, *Adv. Mater.* **2015**, *27*, 5210; b) G. H. Han, H.-J. Shin, E. S. Kim, S. J. Chae, J.-Y. Choi, Y. H. Lee, *Nano* **2011**, *6*, 59.

[13] a) L. G. P. Martins, Y. Song, T. Zeng, M. S. Dresselhaus, J. Kong, P. T. Araujo, *Proc. Natl. Acad. Sci. USA* **2013**, *110*, 17762; b) P. Gupta, P. D. Dongare, S. Grover, S. Dubey, H. Mamgain, A. Bhattacharya, M. M. Deshmukh, *Sci. Rep.* **2014**, *4*, 3882; c) X.-D. Chen, Z.-B. Liu, C.-Y. Zheng, F. Xing, X.-Q. Yan, Y. Chen, J.-G. Tian, *Carbon* **2013**, *56*, 271.

[14] a) B. A. G. Schrauwen, R. P. M. Janssen, L. E. Govaert, H. E. H. Meijer, *Macromolecules* **2004**, *37*, 6069; b) F. Bédouia, J. Diania, G. Régnier, *Polymer* **2004**, *45*, 2433; c) M. Arnoult, E. Dargent, J. F. Mano, *Polymer* **2007**, *48*, 1012.

[15] a) C. Gómez-Navarro, M. Burghard, K. Kern, *Nano Lett.* **2008**, *8*, 2045; b) A. Castellanos-Gomez, M. Poot, G. A. Steele, H. S. J. van der Zant, N. Agraït, G. Rubio-Bollinger, *Adv. Mater.* **2012**, *24*, 772.

[16] a) W. Yan, C. L. Pun, G. P. Simon, *Compos. Sci. Technol.* **2012**, *72*, 1147; b) X. Li, B. Bhushan, *Mater. Charact.* **2002**, *48*, 11.

[17] L. Feng, N. Xie, J. Zhoung, *Materials* **2014**, *7*, 3919.

[18] C. Lee, X. Wei, J. W. Kysar, J. Hone, *Science* **2000**, *321*, 385.

[19] a) S. Chen, L. Brown, M. Levendorf, W. Cai, S.-Y. Ju, J. Edgeworth, X. Li, C. W. Magnuson, A. Velamakanni, R. D. Piner, J. Kang, J. Park, R. S. Ruoff, *ACS Nano* **2011**, *5*, 1321; b) R. Podila, T. Moore, F. Alexis, A. M. Rao, *RSC Adv.* **2013**, *3*, 1660.

[20] G. D. Khattak, A. Mekki, L. E. Wenger, *J. Non. Cryst. Solids* **2004**, *337*, 174.

[21] a) K. Ueno, T. Fukai, T. Nagatsuka, T. Yasuda, M. Watanabe, *Langmuir* **2014**, *30*, 3228; b) J. N. Lee, C. Park, G. M. Whitesides, *Anal. Chem.* **2003**, *75*, 6544; c) B. Ghorani, S. J. Russell, P. Goswami, *Int. J. Polym. Sci.* **2013**, *2013*, 256161.

[22] a) S. Padhi, P. G. R. Achary, N. C. Nayak, *Bull. Mater. Sci.* **2015**, *38*, 925; b) B. Wei, *J. Petrol. Explor. Prod. Technol.* **2015**, *5*, 391.

[23] A. C. Ferrari, J. C. Meyer, V. Scardaci, C. Casiraghi, M. Lazzeri, F. Mauri, S. Piscanec, D. Jiang, K. S. Novoselov, S. Roth, A. K. Geim, *Phys. Rev. Lett.* **2006**, *97*, 187401.

[24] A. Venugopal, J. Chan, X. Li, C. W. Magnuson, W. P. Kirk, L. Colombo, R. S. Ruoff, E. M. Vogel, *J. Appl. Phys.* **2011**, *109*, 104511.

[25] a) A. W. Tsen, L. Brown, M. P. Levendorf, F. Ghahari, P. Y. Huang, R. W. Havener, C. S. Ruiz-Vargas, D. A. Muller, P. Kim, J. Park, *Science* **2012**, *336*, 1143; b) D. V. Tuan, J. Kotakoski, T. Louvet, F. Ortmann, J. C. Meyer, S. Roche, *Nano Lett.* **2013**, *13*, 1730; c) Q. Yu, L. A. Jauregui, W. Wu, R. Colby, J. Tian, Z. Su, H. Cao, Z. Liu, D. Pandey, D. Wei, T. F. Chung, P. Peng, N. P. Guisinger, E. A. Stach, J. Bao, S.-S. Pei, Y. P. Chen, *Nat. Mater.* **2011**, *10*, 443.

[26] a) Y. Zhang, V. W. Brar, C. Girit, A. Zettl, M. F. Crommie, *Nat. Phys.* **2009**, *5*, 722; b) Z. Zhang, H. Xu, H. Zhong, L. M. Peng, *Appl. Phys. Lett.* **2012**, *101*, 213103.

[27] P. L. Levesque, S. S. Sabri, C. M. Aguirre, J. Guillemette, M. Siaj, P. Desjardins, T. Szkopek, R. Martel, *Nano Lett.* **2011**, *11*, 132.

[28] G. Giovannetti, P. A. Khomyakov, G. Brocks, V. M. Karpan, J. van den Brink, P. J. Kelly, *Phys. Rev. Lett.* **2008**, *101*, 026803.

[29] a) M. Ishigami, J. H. Chen, W. G. Cullen, M. S. Fuhrer, E. D. Williams, *Nano Lett.* **2007**, *7*, 1643; b) A. Pirkle, J. Chan, A. Venugopal, D. Hinojos, C. W. Magnuson, S. McDonnell, L. Colombo, E. M. Vogel, R. S. Ruoff, R. M. Wallace, *Appl. Phys. Lett.* **2011**, *99*, 122108.

[30] J. W. Suk, W. H. Lee, J. Lee, H. Chou, R. D. Piner, Y. Hao, D. Akinwande, R. S. Ruoff, *Nano Lett.* **2013**, *13*, 1462.

[31] Y. C. Shin, J. Kong, *Carbon* **2013**, *59*, 439.

[32] S. M. Kim, A. Hsu, Y.-H. Lee, M. Dresselhaus, T. Palacios, K. K. Kim, J. Kong, *Nanotechnology* **2013**, *24*, 365602.

[33] J. Burke, in *Solubility Parameters: Theory and Application*, Vol. *3* (Eds C. Jensen), AIC Book and Paper Group Annual, Washington, D.C. **1984**, pp. 15–58.

[34] Y. Yang, in *Physical Properties of Polymers Handbook*, 2nd ed. (Ed: J. E. Mark), Springer, New York **2007**, pp. 155–163.

[35] S. Franssila, in *Introduction to Microfabrication*, 2nd ed. (Ed: S. Franssila), John Wiley & Sons, Hoboken **2004**, pp 206.

[36] M. Poliskie, *Solar Module Packaging*, CRC Press, **2011**, p. 47.